Compressive Behavior of Orthotropic Steel Deck with Extra Attached Stiffeners

Li, Yongxuan; Liu, Rong; Liu, Yuqing; Xin, Haohui

DOI
10.1061/(ASCE)AS.1943-5525.0000897

Publication date
2018

Document Version
Final published version

Published in
Journal of Aerospace Engineering

Citation (APA)
Li, Y., Liu, R., Liu, Y., & Xin, H. (2018). Compressive Behavior of Orthotropic Steel Deck with Extra Attached Stiffeners. *Journal of Aerospace Engineering*, *31*(6), Article 04018084. https://doi.org/10.1061/(ASCE)AS.1943-5525.0000897

Compressive Behavior of Orthotropic Steel Deck with Extra Attached Stiffeners

Yongxuan Li[1]; Rong Liu[2]; Yuqing Liu[3]; and Haohui Xin[4]

Abstract: The steel stiffened segment in a steel–concrete connection joint is critical to the load capability of the cable-stayed bridge with hybrid girders. The research focused on the improvement of steel stiffened segments by investigating their failure reasons, mechanical behavior, and transmission efficiency. In order to achieve that, both the experiments and finite-element (FE) analysis of three classical types of stiffened segments subjected to axial compression were conducted, and FE results were consistent with test data. Effects of element sizes, geometric imperfections, and residual stresses were considered in FE models, and proper values for the imperfections were suggested. With refined models, transmission efficiency and stress concentration of three types of steel stiffened segments have been investigated. Segments with a U-shaped stiffener inserted T-stiffener and U-shaped stiffener circumscribed double T-stiffener are suggested for better force transmission and less local stress concentration. Furthermore, parameter studies on two suggested types above are carried out. Results show that the vertical plate could be thinning when the condition of stability is satisfied. Proper thickness of the vertical plate in a single T-stiffener and proper spacing between vertical plates in a double T-stiffener are given. **DOI: 10.1061/(ASCE)AS.1943-5525.0000897.**

Author keywords: Steel–concrete composite joint; Buckling; Initial imperfection; Residual stresses; Stress concentration; Force transmission.

Introduction

The hybrid girder system in a cable-stayed bridge, which is composed of the steel girder in the middle span and the prestressed concrete (PC) girders in the side spans, has been widely used in Europe and Japan since it was originally developed in Germany (He et al. 2014). Compared with a concrete girder, a larger span could be achieved by applying the steel girder in the middle span, and compared with a steel girder, the negative reaction at the side pier could be avoided when the concrete girder is utilized in the side span. Moreover, the hybrid girder system has advantages in the stiffness of the side span, the force distribution of cables, and the convenience for construction (Xin et al. 2014). Because of its advantages, more than 26 hybrid cable-stayed bridges with large spans (over 300 m) have been constructed in China since it was first introduced to China in the 1990s.

The steel–concrete connection between two steel girders and a concrete girder is usually composed of the steel stiffened segment, the concrete strengthened segment, and the composite joint, aiming to ensure a stiffness transition and smooth force transmission as shown in Fig. 1. The scheme of the steel stiffened segment is also shown in Fig. 1. In order to achieve a better transition in stiffness in the steel stiffened segment, the reinforcing stiffeners, bearing plates, and extra diaphragms are added into the orthotropic steel deck system. With the help of reinforcing stiffeners, the stress level in deck plates is reduced and the stress concentration between deck plates with U-shaped stiffeners and hybrid joint (steel cell filled with concrete) is decreased. Since the steel–concrete connection is usually near the pylon with great axial forces from cables, the mechanical behavior of each part in the steel–concrete connection under axial compression is crucial to the hybrid girder system, especially the stability of the steel stiffened segment under compression.

Stability of steel structures under axial force has drawn attention for centuries. However, most researchers have focused on the ultimate capacity, the buckling mode, and the failure reason of steel structures with a uniform cross section, while little research has been conducted on structures with stiffeners of variable height. Nevertheless, research methods on the stability of steel structures with a uniform cross section should be learned and adopted. Current research on stiffened steel plate mainly depends on three methods: theoretical analysis, experimental methods, and numerical simulation (Bedair 1998). In terms of the convenience and accuracy of numerical simulation under the development of computer technology, more and more research has been conducted with the finite-element method (FEM), verified by experimental test results.

With the approach of FEM, effects of imperfections, including the residual stresses and geometric imperfections, have been highlighted when accurate simulation and analysis were demanded. Compared with measured results, which are influenced by the material, processing, transportation, test conditions, and methods, the effects of imperfections could be quantified and analyzed in the FE models. Parametric studies considering residual stresses and geometric imperfections on FE models verified by the test results of full-size stiffened plate specimens were conducted by Grondin et al. (1998, 1999). Both the magnitude and the shape of the initial

[1]Doctoral Candidate, Dept. of Bridge Engineering, College of Civil Engineering, Tongji Univ., 1239 Rd., Shanghai 200092, China. ORCID: https://orcid.org/0000-0002-7544-252X. Email: yongxuanli@qq.com

[2]Associate Professor, College of Civil and Transportation Engineering, Hohai Univ., 1 Xikang Rd., Nanjing 210098, China. Email: liurong1002@126.com

[3]Professor, Dept. of Bridge Engineering, College of Civil Engineering, Tongji Univ., 1239 Rd., Shanghai 200092, China (corresponding author). Email: yql@tongji.edu.cn

[4]Postdoctoral Researcher, Faculty of Civil Engineering and Geoscience, Delft 2628, Netherlands. Email: xinhaohui@126.com

Note. This manuscript was submitted on October 3, 2017; approved on March 15, 2018; published online on July 12, 2018. Discussion period open until December 12, 2018; separate discussions must be submitted for individual papers. This paper is part of the ***Journal of Aerospace Engineering***, © ASCE, ISSN 0893-1321.

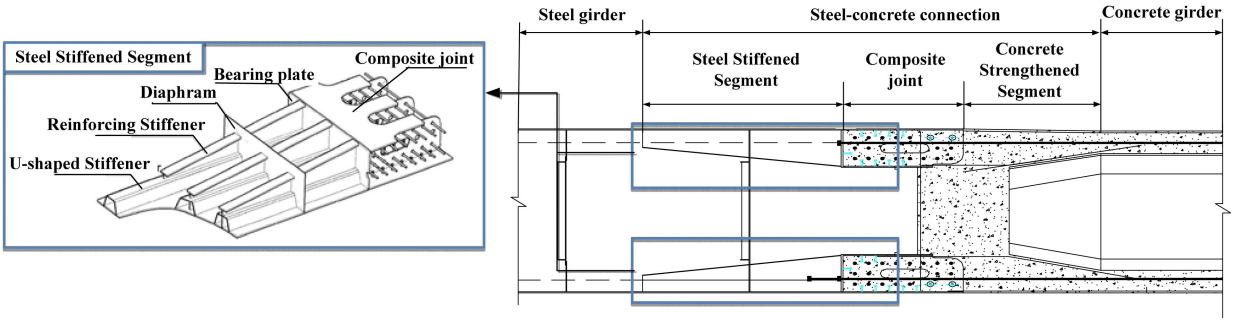

Fig. 1. Scheme of steel concrete connection and steel stiffened segment.

imperfections turned out to have a significant influence on the capacity of stiffened plates. Three half sine waves on the bottom of a U-shaped stiffener were considered as initial imperfections. Chou et al. (2006) conducted tests on two reduced-scale orthotropic plates using ASTM A709 Grade 345 steel to verify the design strength of steel box girders for the new San Francisco–Oakland Bay Bridge. The test results showed that the deck with closed ribs failed in global buckling, followed by local buckling in the deck plate and ribs. With a comparison, the FE model was confirmed as a reliable prediction since models had predicted the capacity and buckling models of both stiffened plates. Zhang and Khan (2009) did a larger numerical simulation of stiffened plates under axial compression by FE models verified by the results of 61 tested stiffened panels. The imperfections were highlighted and applied to structure based on four eigenvalue buckling types of open stiffeners. Shin et al. (2013, 2014) analyzed 112 models with various combinations of slenderness parameters of high-performance steel deck plates to evaluate the prediction in Eurocode. The residual stresses and imperfections were applied to the FE models and weakened the ultimate capacity about 7%. In conclusion, effects of imperfections have been considered in different structures with different materials. Clearly, the effects are negative to the ultimate capacity, leading to an earlier failure. In order to prevent buckling, the residual stress distribution is addressed, such as Federal Highway Administration (FHWA) specifications, and the geometric imperfections are given, such as the AASHTO, FHWA specifications, and Eurocode. However, most standards are concentrated on the design of orthotropic steel decks with U-shaped stiffeners, while the orthotropic steel decks with both the troughs and the reinforcing stiffeners have not been specified. Additional welding accompanies the additional steel plates, resulting in more concentrated residual stresses and larger local deformations. Effects of imperfections need investigating for proper values and the regulations in the standards are compared.

Three classical types of stiffeners in steel stiffened segments are shown in Fig. 2: (1) U-shaped stiffener inserted T-stiffener (IT type), applied in the Edong Yangtze River Bridge with a 926-m main span (Liu et al. 2010); (2) U-shaped stiffener circumscribed single T-stiffener (ST type), applied in the Baishazhou Bridge with a 618-m main span (Wen et al. 1997); and (3) U-shaped stiffener circumscribed double T-stiffener (DT type), applied in the Taoyaomen Bridge with a 580-m main span (Chen et al. 2006). The effects of section change at the end of the reinforcing stiffener were investigated (Liu 2010). The load proportion was utilized to evaluate the force transmission efficiency. In order to investigate the ultimate capacity and the buckling mode of a steel stiffened segment, scaled model tests on three traditional types of stiffeners were carried out by Xin et al. (2014). The results showed that the axial stiffness of IT type stiffeners was the largest while the out-plane stiffness and ultimate capacity were optimal among the three traditional stiffened steel segments. However, the mechanism of the compression stability was not investigated and expressed in detail. Comparison between the different stiffened steel segments should not be evaluated only by the carrying capacity, but also while taking the transmission efficiency into consideration.

Based on the finite-element method, Liu and Liu (2015) used the hot spot stress to suppress stress concentration of three classical types at both ends of the reinforcing stiffeners. The hot spot stress (HSS) method has been widely applied in accurate prediction of stress concentration, which is of primary importance for the fatigue analysis. Finite-element analyses were performed in order to derive the stress concentration factors (SCF) from hot-spot stresses in Kim's research (Kim et al. 2014). The SCF value depends more on joint geometry than the loading type, weld size, type, and location around the weld under consideration. In the research of Liu and Liu (2015), the results showed that the reinforcing dispersed about 50% axial force, and the stress transmission of the joint is improved compared with hybrid structure segments without steel stiffened segments. However, the stress concentration at the front end of the reinforcing stiffener was the reason for the failure of the structure according to the experiment of Xin et al. (2014). The effects of stress concentration on the structure and its influential factors need

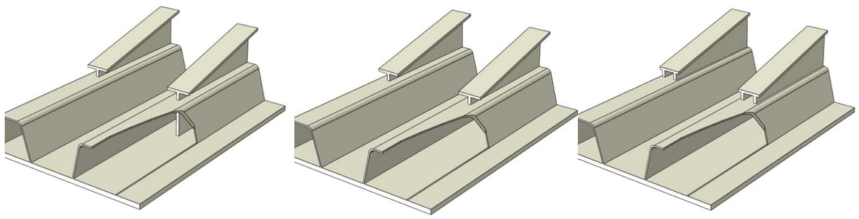

Fig. 2. Three classical types of stiffeners in steel stiffened segments: (a) IT type stiffener; (b) ST type stiffener; and (c) DT type stiffener.

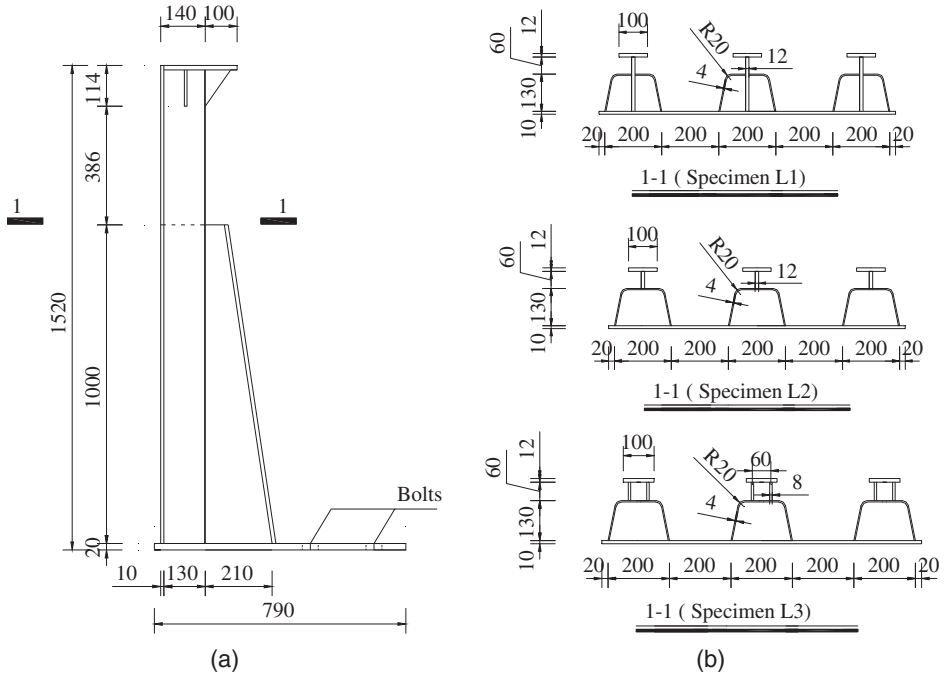

Fig. 3. Details of specimens (in millimeter): (a) side views of specimens; and (b) cross views of specimens.

investigating. The HSS method has been adopted to evaluate the effects of the stress concentration and to discuss the relationship between the capacity and stress concentration.

The objectives of this study were (1) to investigate the mechanical behavior of steel stiffened segments and achieve a better finite-element model validated by experimental data; (2) to figure out the effects of imperfections and proper values for the complex steel stiffened segment; (3) to evaluate the load transmission efficiency and stress concentration of three classical reinforcing stiffeners; and (4) to study the effects of relative plate thickness and relative spacing of reinforcing stiffeners on the whole structure.

In order to investigate the mechanical behavior of steel stiffened segment with three classical sections, shell finite-element models are utilized. Effects of element sizes, residual stresses, and initial imperfections are discussed. Load proportions and transmission efficiency of deck area, U-shaped stiffeners, and reinforcing stiffeners in three specimens are compared with each other in the refined models. The HSS method is used to suppress the stress singularity and to reflect the stress concentration at the suddenly-changed cross section. Effects of relative plate thickness and spacing between vertical plates in double T-stiffeners on the mechanical capability are investigated. The results of this study could not only provide reference for the design and construction of hybrid structures, but also steel structures with variable cross sections.

Experimental Tests

Based on the steel stiffened segment in the Jiujiang Yangtze River Bridge, which is a cable-stayed bridge with a hybrid girder system, scaled tests of three specimens of steel stiffened segments with traditional types were conducted. The similarity ratio of the geometrical dimensions is 1:2. The similarity ratio of the strain, Young's modulus, shear modulus, and Poisson's ratio is 1:1. The similarity ratio of the load is 1:4.

Details of the three half-scale specimens are shown in Fig. 3. An IT type stiffener was adopted in Specimen L1. A ST type stiffener was adopted in Specimen L2. A DT type stiffener was adopted in L3. The side views of the three specimens were the same, while the cross view showed the differences of the reinforcing stiffeners. Each specimen was composed of three stiffeners. The length of the deck and U-shaped stiffeners stiffened along the deck was 1,520 mm. The width of the deck was 1,040 mm and the thickness was 10 mm. The height of the end bearing plate was 790 mm and the thickness was 14 mm. The length of the single T-stiffeners was 1,000 mm and the thickness was 12 mm. The height of a vertical plate in the single T-stiffener at the end bearing plate was 350 mm and the skew angle was 8.5°. In order to avoid local buckling of stiffeners at the end bearing plate, the triangle stiffeners were added to U-shaped stiffeners. Material tests of each plate were listed in Table 1.

The tests were carried out in the Structure Laboratory of Tongji University and the test system is shown in Fig. 4. Three specimens were anchored by bolts to the ground at one side, while the other end was connected with the actuators of the hydraulic servo system, limited to 20,000 kN. The entire structure was under the vertical pressure provided by the hydraulic servo system to imitate the load carrying of steel stiffened segments under the axial force. Vertical,

Table 1. Material tests of the steel plates

Plate	Thickness (t_m/mm)	Yield strength (f_y/MPa)	Tensile strength (f_y/MPa)	Young's modulus (E/GPa)
Deck	10	365	505	204
U-shaped stiffener	4	425	555	205
Vertical single T-stiffener	12	380	535	204
Horizontal single T-stiffener	12	360	515	204
Vertical double T-stiffener	8	425	520	205
Horizontal double T-stiffener	8	350	510	205
End bearing plate	14	—	—	—

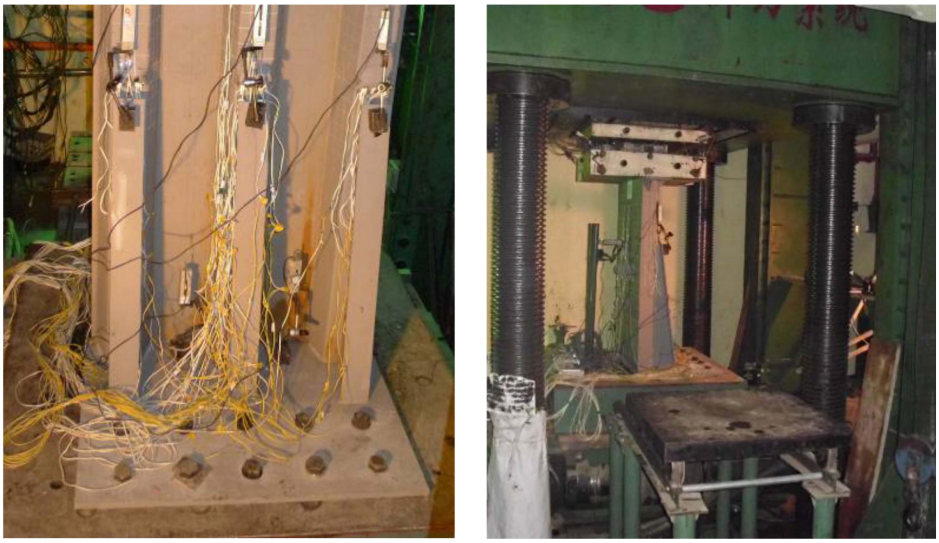

(a) (b)

Fig. 4. Test system: (a) anchorage bolts; and (b) testing device.

horizontal, and local buckling deformation was measured by linear variable displacement transducers. Strains in the deck and stiffeners were measured by gauges.

Finite-Element Analysis

Finite-Element Model

The shell model of the specimen was built with FE modeling software ANSYS Version 14.5 to analyze the deck model. Element SHELL181 with four nodes and the linear shape function was utilized since it was well suited for linear, large rotation, and large strain nonlinear applications, not only owing to good performance in the analysis on the bending of plate and membrane mechanics behavior, but also as a result of consideration of shear deformation. In the element domain, full integration was employed in nonlinear applications. Each node of the element had 6 degrees of freedom: the translations in the local X, Y, and Z directions and rotations in the local X, Y, and Z axes. The thickness was given by real constant data. The boundary condition of the FE model was shown in Fig. 5. The nodes on the end bearing plate were fixed in all directions to simulate the ground constraint and the nodes on the top end plate were constrained as a rigid region with incremental vertical displacements to simulate the displacement loads. The transverse and out-of-plane displacements of the top end plate were constrained. The shapes of shell elements are rectangular and the aspect ratio of the element is close to 1.0 for better calculation. Element size at the end of stiffener was refined to study the mechanical behavior and stress concentration, shown in Fig. 5 was refined to study the mechanical behavior and stress concentration with a better simulation.

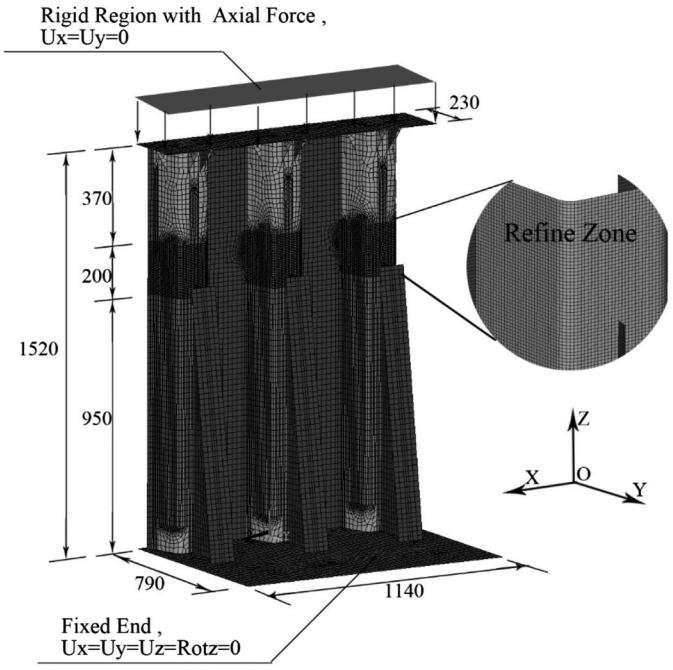

Fig. 5. Finite-element discretization and the boundary condition (in millimeter).

Effects of Element Size

In order to build the FE model accurately, effects of element size, residual stresses, local and global imperfections were investigated in the FE model of Specimen L1. The same values of these factors were applied to the other two specimens.

Effects of element size are shown in Fig. 6. The effects are more focused on the area not in the refined region since the mesh density in the refined region is required by the stress concentration and shown in "Stress Concentration in the U-Shape Stiffener." e is the element length and t is the plate thickness. In general, the ultimate capacity decreases as the element mesh density increases. However, when e/t is about 2.0 and even smaller than 2.0, the ultimate capacities remained about the same, and errors between the FE model result and tests are limited to 2%. Mechanical behavior of the specimen could be simulated more accurately with an element size that is twice that of each plate thickness.

Effects of Residual Stresses

Effects of residual stresses on the steel structure under axial compression have drawn attention. Grondin et al. (1998) assumed

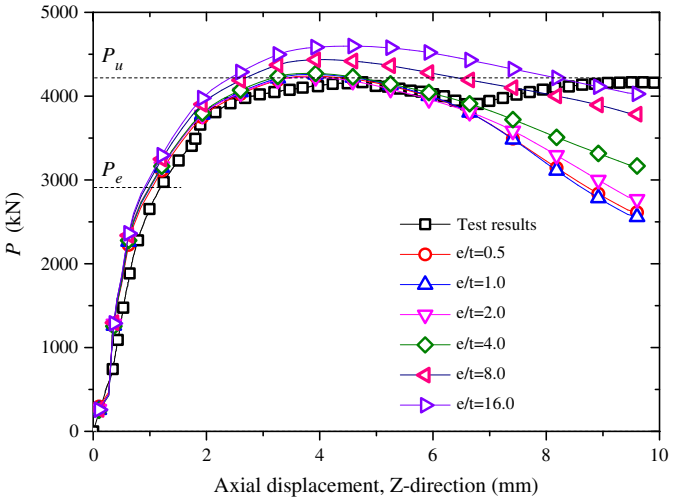

Fig. 6. Effects of element size.

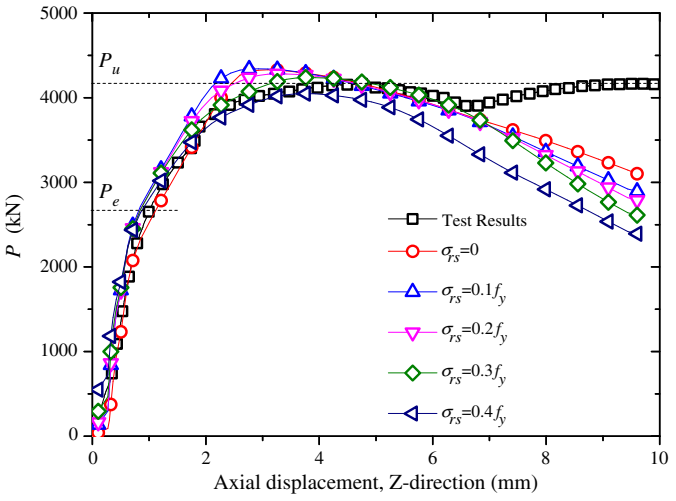

Fig. 8. Effects of residual stresses.

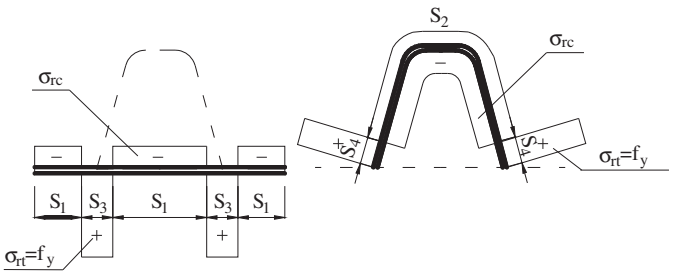

Fig. 7. Idealized distribution of residual stresses.

residual compressive stress as $0.15f_y$ and the effects were less related to the capability. However, Chou et al. (2006) used a nonlinear finite-element analysis, and both the effects of the residual stresses (taking $0.25f_y$ as the residual compressive stress) and initial geometric imperfections were considered. The results showed that the residual stresses lead to a decline of the capacity and impact the behavior in the elastoplastic stage. Jen and Yen (2006) used the uniformly idealized residual compressive stress with $0.2f_y$ for the deck panel and $0.1f_y$ for the rib wall. The predicted ultimate load was about 14% higher than the test results. Shin et al. (2013) introduced an ideal residual stress distribution of ordinary steel proposed in Section 4.8.3 in FHWA (2012) to the plates with U-shaped stiffeners. A better simulation and capacity estimate were achieved with a 7% decline in ultimate capacity when the imperfections and the residual stresses were considered in the model. Furthermore, the residual stresses were the main reason for the decline. Based on the reliability theory, Duc et al. (2013) used Monte Carlo simulation and a large number of deterministic FEM to analyze the influential factors of local buckling stress. The mean of residual compressive stress was $0.232f_y$ according to over 220 residual stress test results. The magnitude of stress could be quite different due to welding methods, materials, processes, pretreatments, and post-treatments. In order to achieve a better FE model, the effects of residual stresses are discussed.

The distribution of residual stresses was assumed to be similar to the self-equilibrating stress pattern suggested by FHWA (2012), as shown in Fig. 7. σ_{rc} is residual stress in the compressive zone and σ_{rt} is that in the tension zone. S_1 and S_2 are the length of the deck and U-shaped stiffeners with residual tension stress, while S_3 and S_4 are those with residual compressive stress. Since σ_{rt} was assumed as f_y constantly, S1–S4 varied with σ_{rc}. Since the residual stress is self-balanced, Eq. (1) must be satisfied, as follows:

$$\sum_{i=1}^{2} S_i\sigma_{rc} + \sum_{i=3}^{4} S_i\sigma_{rt} = 0 \tag{1}$$

Effects of residual stresses are shown in Fig. 8. The ultimate capacity P_u decreased 4.5% as σ_{rc} increased. At the same time, the displacement response of ultimate capacity increased. The ductility of the structure was improved and more consistent with the experiment results. Residual compressive stress governed the plastic behavior of structure and elastic capability P_e. Mechanical behavior of the specimens could be simulated more accurately with $\sigma_{rc} = 0.3f_y$.

Effects of Geometric Imperfections

Effects of residual initial imperfections are shown in Fig. 9. Initial imperfections are comprised of global imperfections and local imperfections.

For global imperfection shown in Fig. 9(a), Δ/L is discussed as a parameter, where Δ refers to the out-plane displacement at the sudden-changed cross section and L refers to the length of the specimen. Part 1-1 of Eurocode 3 (CEN 2006a) suggested that the global initial imperfections should be taken as approximately 1/100–1/250 in nonlinear finite-element analysis, depending on the properties of cross sections, while 1/1,000 is the suggestion in FHWA (2010) for steel structures. For steel stiffened segments in this research, the cross section changes all the time. Moreover, the residual stress was more concentrated at the sudden-changed cross section due to welding. It could be indicated that the global imperfections mainly affect the axial stiffness of the structure and the ultimate capacity P_u. Compared with residual stresses that are also related to the ultimate capacity, global imperfections have a minor influence on the ductility. The larger the global imperfections are, the more the axial stiffness declines. The results show a good agreement with a model with a Δ/L of about 1/125, which also satisfies Table 5.1 in Part 1-5 of Eurocode 3 (CEN 2006b).

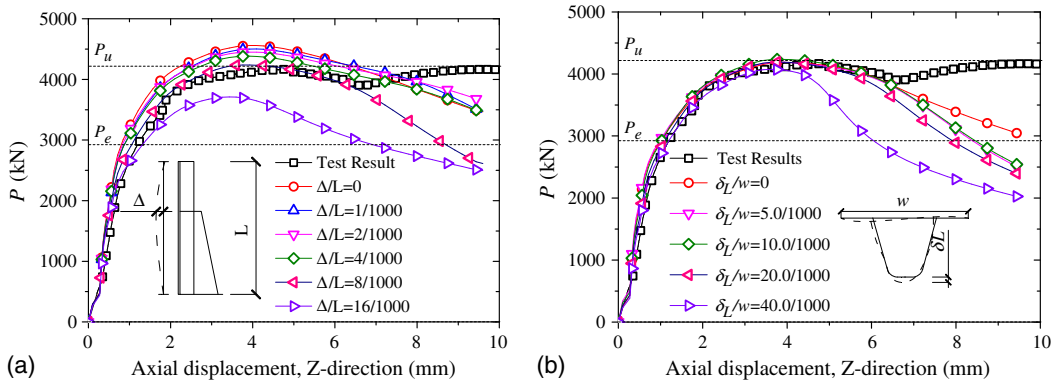

Fig. 9. Effects of initial imperfections: (a) effects of global imperfections; and (b) effects of local imperfections.

For the local imperfection shown in Fig. 9(b), δ_L/w was considered as the parameter, where δ_L refers to the out-plane displacement at the surface of the U-stiffener and w refers to the deck spacing between stiffeners. Eurocode (CEN 2006b) suggested that the initial local imperfections should be taken as 1/200 in nonlinear FE analysis based on the buckling shape calculated by an elastic eigenvalue buckling analysis. The local imperfections mainly affect the postbuckling area. The larger the local imperfections are, the faster the ultimate capacity P_u declines. Effects of local imperfections to mechanical behavior are negligible. The results show a good agreement with the model with a δ_L/w of about 1/200, which also satisfies Table C.2 in Eurocode 3 (CEN 2006b).

Compression Mechanism of the Steel Stiffened Segment

Verification of Finite-Element Model

With appropriate values of element size, residual stresses, and initial imperfections, the whole failure process was analyzed by FE models with the same approach. The ultimate capacity, axial stiffness, and buckling mode of FEM results are compared with experimental data.

The load-displacement curves of three specimens are presented in Fig. 10. The whole process of the structure under axial

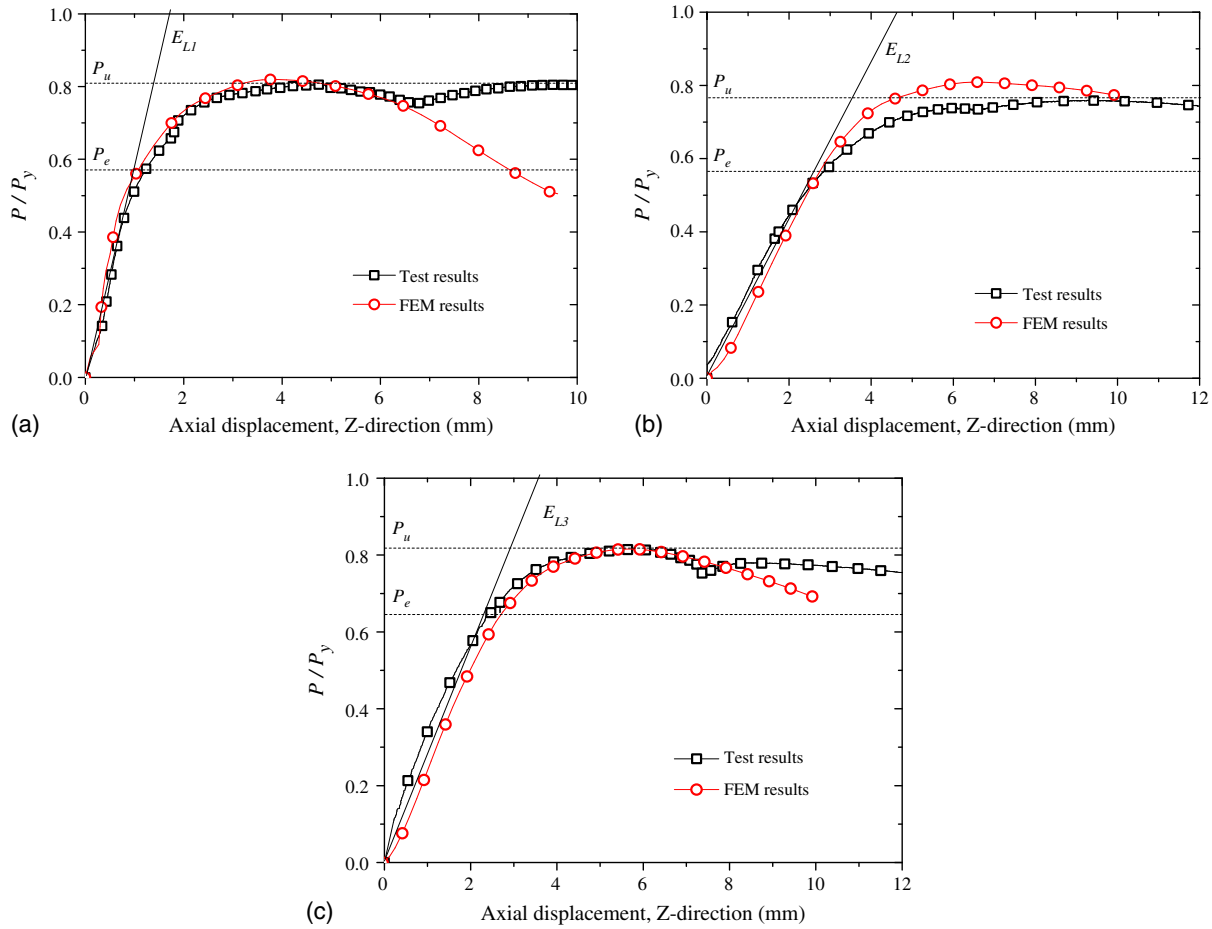

Fig. 10. Load-displacement curve: (a) Specimen L1; (b) Specimen L2; and (c) Specimen L3.

J. Aerosp. Eng., 2018, 31(6): 04018084

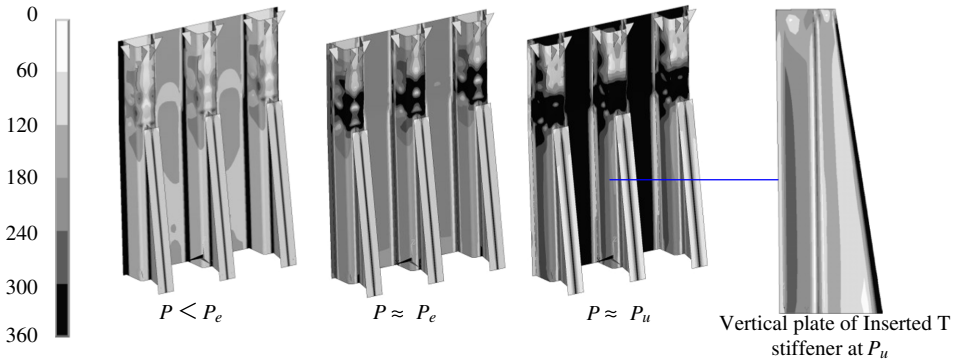

Fig. 11. Stress distribution of Specimen L1 under compression.

compression is composed of three stages that are the elastic stage, the plastic stage, and the postbuckling stage.

P_e and P_u in Fig. 10 refer to the elastic and ultimate capacity of specimens, respectively. P_y refers to the yielding capacity with minimum area of the structure, equal to $f_y \times A$. f_y is the yield strength of the steel material and A is the minimum cross-sectional area of the structure, which is the cross section without reinforced stiffeners, and the area is about 14,991 mm^2. Also, f_y is about 365 MPa. So, $P_y = f_y \times A \approx 5{,}175$ kN.

P_u of L1 and L3 are 7% higher than that of L2, while P_e values of the three specimens are similar. The IT type stiffener and circumscribed double T-stiffener can provide a larger ultimate capacity. The FEM results show a great agreement with all experimental data in all stages. The error between the ultimate capacity of FEM results and test results on three specimens is lower than 5%, satisfying the engineering requirement.

E_{L1-3} in Fig. 10 refers to the initial axial stiffness of specimens. As results show that $E_{L1} > E_{L3} > E_{L2}$, IT type stiffeners provide the best axial stiffness and DT type stiffeners come second. The axial stiffness of the FEM is also similar to the test results.

Mechanical Behavior of Specimens

Fig. 11 shows the von Mises stress distribution of Specimen L1 in the whole process. At the elastic stage, the stress of the whole structure is in a lower range except for the bottom plate of the U-stiffener due to a great initial geometric default and the compressive residual stress. When P reaches P_e, the entire bottom of the U-stiffener yields. Part of the side wall of the U-stiffener also yields at the same time. As the load continues increasing, the stress of the deck plate increases and the whole section yields as the load reaches P_u. The vertical plate of the inserted T-stiffener does not yield, even when reaching the ultimate load, as shown in the figure, which indicates that the buckling at the U-stiffener is the failure reason of the whole steel stiffened segment. The stress distribution in the vertical plate is striplike. The stress in the vertical plate of the T-stiffener near the deck plate reaches yield strength, and the stress decreases as the distance to the deck increases.

Fig. 12 shows the plastic strain of the feature point of the same cross section in each part as the load increases. When the bottom of the U-stiffener yields, the stiffness of the whole structure remains the same, indicating that the bottom of the U-stiffener has a minor effect on the elastic capacity. Once the side wall of the U-stiffener yields, the load reaches P_e and the stiffness of the segment decreases, indicating that the plastic behavior of the side wall controls the elastic capacity. The yielding of the deck with compressive stress follows, while the deck plate with tensile residual stress does not come to yield until the applied load reaches P_u.

The out-of-plane displacement of the U-stiffener with the applied load variation is shown in Fig. 13. The bottom of the U-stiffener wall results in convex deformation away from the initial flat position and the side walls result in concave deformation. The buckling displacement of the side wall begins when the load reaches P_e. The out of plate displacement increases sharply due to buckling when it comes to the ultimate load P_u. Clearly, yield of the side wall in the U-shaped stiffener decreases the stiffness and

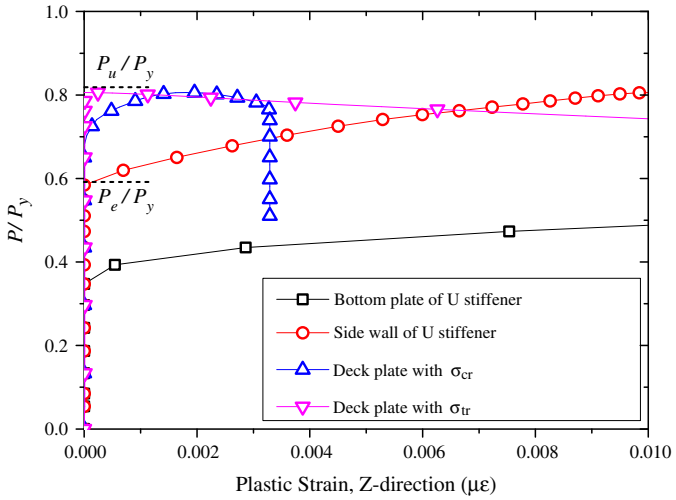

Fig. 12. Plastic strain of each part in the same cross section.

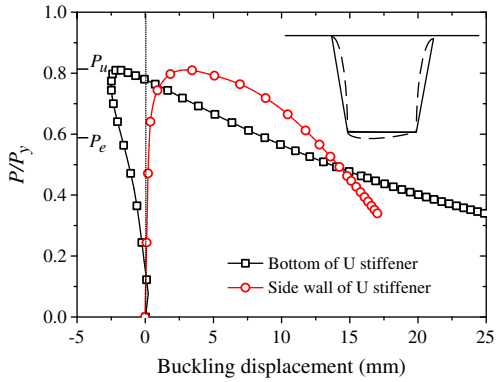

Fig. 13. Buckling displacement of the U-stiffener.

Fig. 14. Buckling failure of Specimen L1.

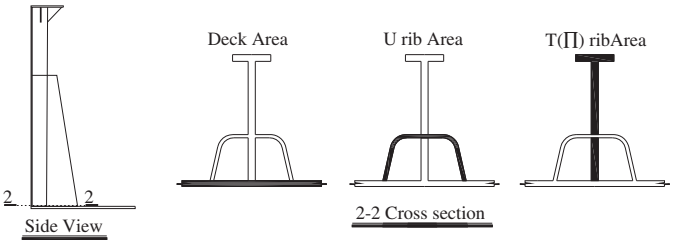

Fig. 15. Position of Section 2-2 and three parts in the section.

induces the buckling of the U-shaped stiffener, which leads to the failure of the structure.

Since the buckling behaviors of the three specimens are similar to one another, the buckling failure mode of Specimen L1 subjected to axial compression is shown in Fig. 14. The convex deformation of the U-rib bottom wall and the concave deformation of the U-rib side wall show that the steel stiffened segment suffered local buckling. Since the buckling area was mainly in the region of the U-shaped stiffeners at the end of a single T-stiffener, the reason for the local buckling of Specimen L1 was the stress concentration due to the sudden change between cross sections. The failure area and buckling mode of the FEM are consistent with test results.

Transmission Efficiency of Three Classic Segments

The main purpose of steel stiffened segment in a hybrid joint is to ensure a stiffness transition and smooth force transmission. Suppose that the cross section at the end of the steel stiffened segment had been divided into several parts. If the force were transferred long enough, the section stress would be the same. Therefore, the load proportion in each part of the section would be the same as the area proportion of each part under compression.

However, the inertia moment of the section is not the same among the three specimens in terms of the section properties. In terms of external force conditions, the center of force is changing along with the variable height and increased load. Moreover, the length of the steel stiffened segments is usually limited between diaphragms in reality. The length of the current specimen is 1,000 mm.

In order to evaluate the transmission efficiency of a steel stiffened segment, the load distribution in the Cross Section 2-2 was discussed. The 2-2 cross section is shown in Fig. 15. Yielding and buckling did not occur in Section 2-2 in the whole process. In the 2-2 section, the region is divided into three parts: the deck area, the U-rib area, and the T-rib (or Π-rib) area, which are indicated by a black color in each diagram.

Load proportions in each part of the three specimens with load varying from zero to P_u are shown in Fig. 16. The dashed lines in each figure show their area proportions, with squares for Specimen L1, circles for Specimen L2, and triangles for Specimen L3. The deck area takes most of the load compared with other parts.

Fig. 16(a) shows the load proportions of the deck area with load variation. The main results are as follows: (1) The area proportions of the deck area among the three specimens are similar to one another, while the load proportions are different, but generally, a higher load proportion is taken by a larger area proportion. (2) As the load increases, the load proportions grow slowly. (3) The load proportions are higher than the area proportions. Therefore, the deck is still the main part for force transmission. (4) The load proportion of the deck of L1 is lowest among three specimens, indicating that the IT type stiffener provides a better force transmission as more load is carried by the other parts of the section.

Fig. 16(b) presents the load proportions of the U-rib area. The main results are presented: (1) Unlike the deck area, although the area proportions of the U-rib area are similar to each other, the highest load proportion is taken by the deck with the DT type stiffener. (2) As the load increases, the load proportions are growing slowly generally. Comparatively, the U-rib area of L3 shows a stable behavior. (3) The load proportions of L3 are close to the area proportions, while the other two are lower, indicating that the U-rib area of L3 may be better stiffened with a DT type stiffener.

The load proportions of the T-rib or Π-rib area are shown in Fig. 16(c). From the figure, it can be concluded that (1) like the deck area, a higher load proportion is taken by a higher area proportion; (2) as the load increases, the load proportions are gradually decreasing; (3) the load proportions are much lower than the area proportions; and (4) the load proportion of L1 is much higher than the other two specimens, owing to the vertical plate inside the U-shaped stiffeners. The circumscribed stiffeners provide a bad performance in force transferring compared with the inserted stiffeners.

It can be concluded that the sections with IT type stiffeners (applied in Specimen L1) and DT type stiffeners (applied in Specimen L3) have advantages in reducing the stress level in the deck. The axial force of the deck in L1 is transferred to the reinforcing stiffener, because the U-shaped stiffener is reinforced on both sides. The axial force of the deck in L3 is transferred to the U-shaped stiffener since the bottom plate of the U-shaped stiffener is better stiffened by the two vertical plates, albeit reinforced on only one side. Both the section inserted T-stiffener and circumscribed double T-stiffener are suggested in practice.

Stress Concentration in the U-Shaped Stiffener

Local buckling occurs in the structure first, and it is accompanied by the global buckling of the whole structure, leading to failure. The reason for local buckling is local stress concentration in the bottom plate of the U-shaped stiffener.

Since Liu's work (2015) proved that the stress results of models with a coarse mesh of one layer with an eight-node element were less than 5% lower than the results of refined models with a mesh of six layers through the plate thickness. The shell element was used to build the model to simplify the calculation while ensuring accuracy. Similar to the FEM of specimens, shell element SHELL181 was utilized in the analysis. A refined mesh with $e/t = 0.2$ is applied to the position of most concern.

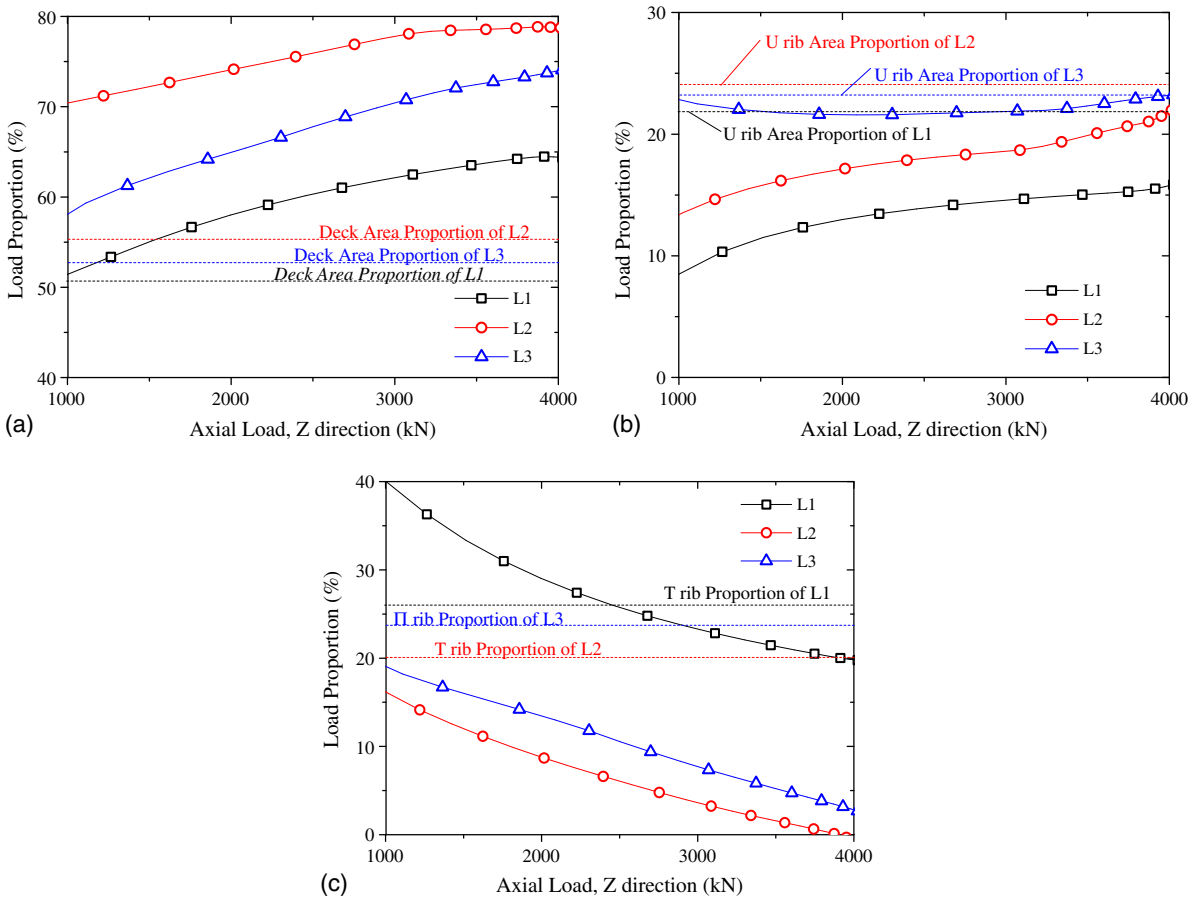

Fig. 16. Load proportions in cross section with load variations: (a) deck area; (b) U-rib area; and (c) T-rib (Π-rib) area.

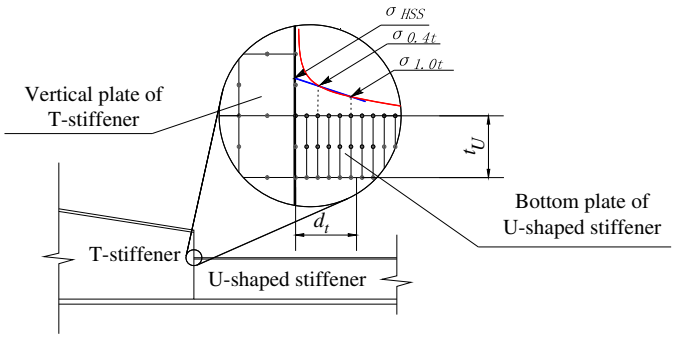

Fig. 17. Hot spot stress and the reference stress point at the end of a single T-stiffener.

The structure is based on the following assumptions:

1. The whole cross section of a U-shaped stiffener is under uniform axial compressive force without eccentricity;
2. The elastic behavior is considered only; and
3. The structure is analyzed without considering the residual stresses and initial imperfections.

To suppress the stress singularity and to reflect the stress concentration of the joint, the HSS method specified by the International Institute of Welding (Hobbacher 2016) was taken, as shown in Fig. 17. d_t represents the distance to the sudden-change cross section and t_U is the thickness of the U-shaped stiffener. The actual stress is presented by the solid lines, while the dotted lines refer to the hot spot stress calculated as the difference between $\sigma_{0.4t}$ and $\sigma_{1.0t}$, where $\sigma_{0.4t}$ and $\sigma_{1.0t}$ are reference stresses.

Stress concentration factor K_t is defined as follows:

$$K_t = \frac{\sigma_{HSS}}{\sigma_{nom}} \tag{2}$$

where σ_{HSS} refers to the HSS and σ_{nom} refers to the nominal stress of the whole cross section.

Stress concentration at the bottom of the U-shaped stiffener in three typical cross sections is presented in Fig. 18. d is the distance to the end of the T-stiffener (or Π-stiffener) and t is the thickness of the U-shaped stiffener. K_t goes down as the distance to the sudden-changed section increases. The K_t of L1, L2, and L3 is 7.8, 9.3, and 7.4, respectively. The ST type stiffener shows a bad mechanical behavior as the K_t of L2 is significantly higher than those of L1 and L3. The K_t values of L1 and L3 are close to each other. The local structures of L2 and L3 are similar, while the stress concentration in ST type stiffeners is more serious than that in the DT type. The higher the stress concentration factor is, the smaller the ultimate capacity. The structure of the DT type stiffener is similar to the ST type stiffener in the local region, which is composed of a vertical plate welded to the bottom of the U-stiffener. However, the discrepancy of the stress concentration factor of this region is significant. The reason needs to be investigated.

Parameter Analysis on Steel Stiffened Segment

It could be indicated that Specimens L2 and L3 have advantages in application for better force transmission and less local stress concentration. However, the mechanical behavior of the structure is

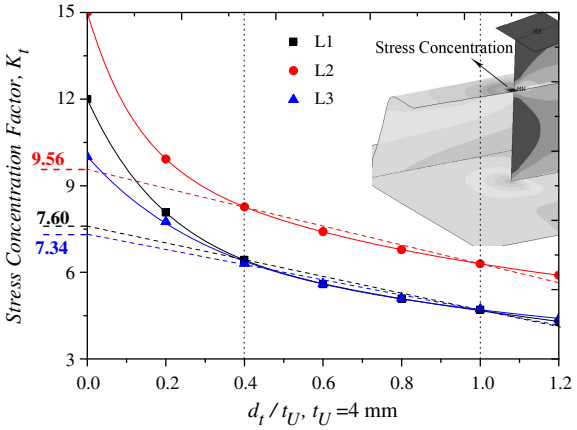

Fig. 18. Stress concentration of three types of cross sections.

greatly related to the geometric size of the structure. The vertical plate thickness and the spacing between vertical plates in double T-stiffeners are discussed as the main influential factor of the reinforcing stiffeners since the deck and U-shaped stiffeners are usually determined by the global response of the bridge.

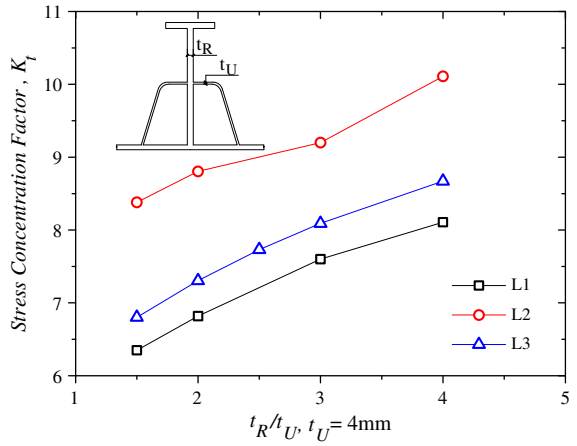

Fig. 19. Effects of plate thickness on stress concentration.

Effects of Vertical Plate Thickness

Effects of plate thickness on stress concentration are shown in Fig. 19. Since stress concentration is mainly related to the structure, the relative thickness of t_R/t_U is discussed, where t_U is the thickness of the U-shaped stiffness, equal to 4 mm constantly, and t_R is the thickness of the vertical plate in reinforcing stiffness, illustrated in Fig. 19. K_t is sensitive to the thickness and the stress concentration rises up as the vertical plate thickens, generally. In order to improve the local stress concentration of a reinforcing stiffener at the elastic stage, the relative thickness could be reduced in a proper range considering plate buckling.

Effects of plate thickness on the load proportions with load variation are shown in Fig. 20. Generally, the load proportion in the U-rib area remains almost the same, while that in the T-rib area clearly increases as the vertical plates thicken, indicating a lower stress level in the deck. In order to improve the load proportion of a reinforcing stiffener at the elastic stage, the vertical plate thickness could be increased for U-shaped stiffener circumscribed stiffeners. While for an IT type stiffener, when t_R/t_U is between 2 and 3, the plate thickness could be reduced at a certain level due to a minor difference. The inserted vertical plate buckles when the thickness of the vertical plate is too thin. Buckling of the inserted plate needs to be prevented.

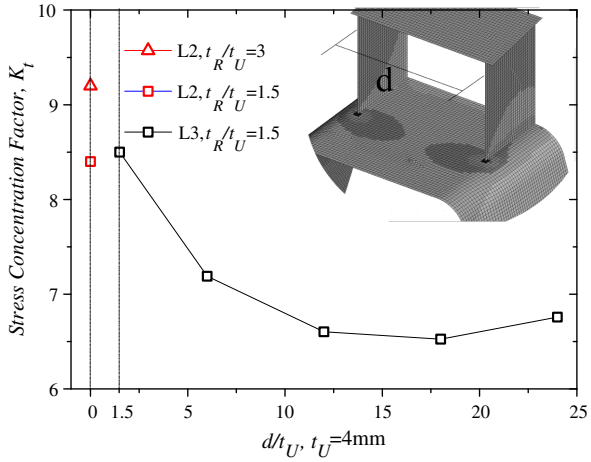

Fig. 21. Effects of spacing between vertical plates on stress concentration.

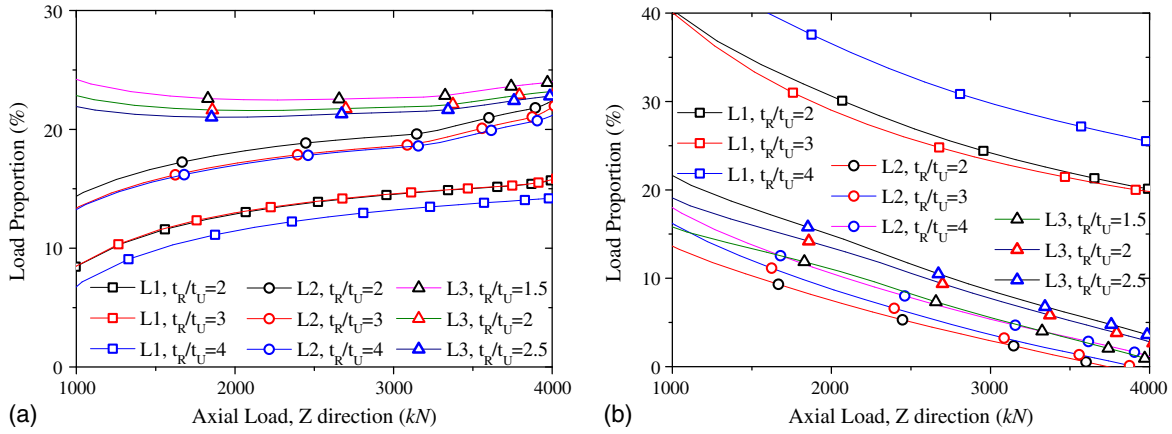

Fig. 20. Effects of plate thickness on the load proportions with load variation: (a) U-rib area; and (b) T-rib (II-rib) area.

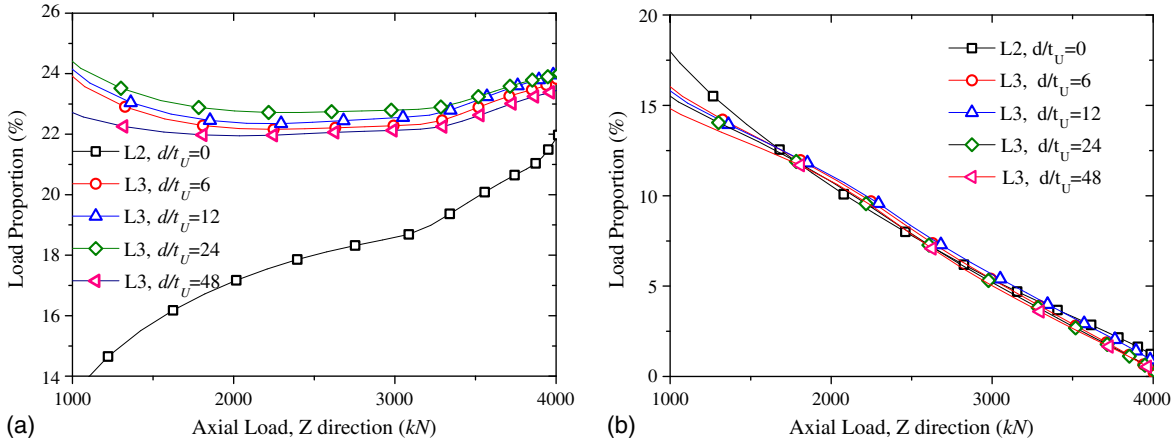

Fig. 22. Effects of spacing between vertical plates on load proportions: (a) U-shaped stiffener; and (b) T (Π) stiffener.

Effects of Spacing between Vertical Plates

As shown in Fig. 3, a double T-stiffener contains two vertical plates of 8-mm thickness, while a single T-stiffener contains one vertical plate with a thickness of 12 mm. In order to investigate the effects of spacing between vertical plates with a single variable, 6-mm-thick vertical plates in a double T-stiffener were applied in FE models for L3 in Section 5.2.

Effects of spacing between vertical plates on stress concentration are presented in Fig. 21. d refers to the distance of spacing. The stress concentration factor K_t increases at first and then decreases as the spacing enlarges. When the vertical plates are attached tightly, which means $d/t_U = 1.5$, a close result is presented between L2 and L3 with the same thickness of a single plate. If the vertical plates are welded far from each other, which means d/t_U is large enough, K_t would also be around 8.5. When the spacing is between these two extreme cases, K_t could be decreased to 6.5 with a proper spacing. The distance of spacing from $12t_U$ to $16t_U$ is suggested in practice to avoid local stress concentration, since the local stress concentration is weakened by a more effective area in the bottom of the U-shaped stiffener. The larger effective area is also the reason for a more stable load proportion in a DT type stiffener with load variation.

Effects of spacing between vertical plates on load proportions are shown in Fig. 22. The spacing has a negligible influence on load proportions in reinforcing stiffeners. The load proportions in the U-rib area increase with increasing spacing within a proper range. If the spacing continues to increase, the load proportions decrease, since the positive effects of the two vertical plates on the bottom plate of the U-shaped stiffener are weakened. The stiffeners could share more load with a proper spacing from $12t_U$ to $24t_U$.

Conclusions

Compressive behavior of steel stiffened segments was investigated by experimental tests and finite-element models. The following results have been obtained:

1. Based on an analysis of the refined FEM of segments, yield of the side wall in the U-shaped stiffener decreases the stiffness and induces the buckling of the U-shaped stiffener, which leads to the failure of the structure. Compared with $1/1{,}000$ and $0.25f_y$ suggested in the FHWA standard for steel structures, larger initial imperfections and greater residual stresses should be considered in the analysis on structures with sudden-change cross sections and much welding.
2. Segments with IT and DT type stiffeners are suggested for better force transmission and less local stress concentration. The axial force of the deck in the former one is transferred to the reinforcing stiffener due to the stiffener plate inside the U-shaped stiffener, while in the second one it is transferred to the U-shaped stiffener owing to the bottom and side walls of the U-shaped stiffener, which is better stiffened by the two vertical plates.
3. For IT type stiffeners, the force transmission behaviors are almost the same as the thickness changing, while the stress on the bottom of the U-stiffener is concentrated with vertical plate thickening. Thereby, the vertical plate could be thinning in the condition of stability satisfied, and $2t_U$ to $3t_U$ is suggested as the thickness of the vertical plate.
4. For DT type stiffeners, the local stress concentration could be weakened due to a more effective area of the U-shaped stiffener when spacing increases in a certain rage. Also, it could be indicated that the spacing has a negligible impact on force smooth transition. Therefore, the distance of spacing between vertical plates of double T-stiffeners from $12t_U$ to $16t_U$ is suggested in practice.

Acknowledgments

The research reported herein has been carried out as part of the research projects granted by the National Natural Science Foundation of China (51108153). This paper is also partly supported by Fundamental Research Funds for National Universities (B12020019). Assistance from both is gratefully acknowledged. The authors thank the editors and the referees for their detailed comments that have helped improve this paper substantially.

References

Bedair, O. K. 1998. "A contribution to the stability of stiffened plates under uniform compression." *Comput. Struct.* 66 (5): 535–570. https://doi.org/10.1016/S0045-7949(97)00102-8.

CEN (European Committee for Standardization). 2006a. *Eurocode3: Design of steel structure: Part 1-1: General rules and rules for buildings*. BS-EN 1993-1-1:2005. Brussels, Belgium: CEN.

CEN (European Committee for Standardization). 2006b. *Eurocode3: Design of steel structure: Part 1-5: Plated structural elements*. BS-EN 1993-1-5:2006. Brussels, Belgium: CEN.

Chen, K. L., J. Z. Wang, and H. Q. An. 2006. "Experimental study on steel-concrete composite join of Zhoushan Taoyaomen Bridge." [In Chinese.] *Chin. J. Civ. Eng.* 3: 86–90. https://doi.org/10.15951/j.tmgcxb.2006.03.013.

Chou, C. C., C. M. Uang, and F. Seible. 2006. "Experimental evaluation of compressive behavior of orthotropic steel plates for the new San Francisco-Oakland Bay Bridge." *J. Bridge Eng.* 11 (2): 140–150. https://doi.org/10.1061/(ASCE)1084-0702(2006)11:2(140).

Duc, D. V., Y. Okui, K. Hagiwara, and M. Nagai. 2013. "Probabilistic distributions of plate buckling strength for normal and bridge high-performance steels." *Int. J. Steel Struct.* 13 (3): 557–567. https://doi.org/10.1007/s13296-013-3014-1.

FHWA (Federal Highway Administration). 2012. *Manual for design, construction, and maintenance of orthotropic steel deck bridges*. Washington, DC: US Dept. of Transportation.

Grondin, G. Y., Q. Chen, A. E. Elwi, and J. J. R. Cheng. 1998. "Stiffened steel plates under compression and bending." *J. Constr. Steel Res.* 45 (2): 125–148. https://doi.org/10.1016/S0143-974X(97)00058-8.

Grondin, G. Y., A. E. Elwi, and J. J. R. Cheng. 1999. "Buckling of stiffened steel plates—A parametric study." *J. Constr. Steel Res.* 50 (2): 151–175. https://doi.org/10.1016/S0143-974X(98)00242-9.

He, J., Y. Q. Liu, and B. Pei. 2014. "Experimental study of the steel-concrete connection in hybrid cable-stayed bridges." *J. Perform. Constr. Facil.* 28 (3): 559–570. https://doi.org/10.1061/(ASCE)CF.1943-5509.0000444.

Hobbacher, A. F. 2016. *Recommendations for fatigue design of welded joints and components: Commission IIW-2259-15*. 2nd ed. New York: International Institute of Welding.

Jen, W. C., and B. T. Yen. 2006. *Load carrying capacity of steel orthotropic deck panel with trapezoidal shaped longitudinal stiffeners*. ATLSS Rep. No. 06-15. Bethlehem, PA: Lehigh Univ.

Kim, I., C. Chung, C. Shim, and Y. Kim. 2014. "Stress concentration factors of N-joints of concrete-filled tubes subjected to axial loads." *Int. J. Steel Struct.* 14 (1): 1–11. https://doi.org/10.1007/s13296-014-1001-9.

Liu, R. 2010. "Rational design of steel-concrete connection in hybrid girder of cable-stayed bridge." [In Chinese.] Ph.D. thesis, Dept. of Bridge Engineering, Tongji Univ.

Liu, R., and Y. Q. Liu. 2015. "Analysis of auxiliary ribs in steel-concrete joint of hybrid girder." *J. Constr. Steel Res.* 112: 363–372. https://doi.org/10.1016/j.jcsr.2015.05.015.

Liu, R., J. L. Yu, Y. Q. Liu, and D. J. Wu. 2010. "Mechanical analysis of joint in steel-concrete hybrid girder of Edong Yangtze River Bridge." [In Chinese.] *Chin. Bridge Constr.* 3: 33–35.

Shin, D. K., B. V. Dat, and K. Kim. 2014. "Compressive strength of HPS box girder flanges stiffened with open ribs." *J. Constr. Steel Res.* 95 (4): 230–241. https://doi.org/10.1016/j.jcsr.2013.12.014.

Shin, D. K., V. A. Le, and K. Kim. 2013. "In-plane ultimate compressive strengths of HPS deck panel system stiffened with U-shaped ribs." *Thin-Walled Struct.* 63: 70–81. https://doi.org/10.1016/j.tws.2012.10.001.

Wen, W. S., S. Y. Wang, and B. M. Wang. 1997. "Research on joint of hybrid girder in cable-stayed bridge." [In Chinese.] *Chin. J. Bridge Eng.* 3: 75–81.

Xin, H. H., Y. Q. Liu, J. He, and Y. Y. Zhang. 2014. "Experimental and analytical study on stiffened steel segment of hybrid structure." *J. Constr. Steel Res.* 100 (13): 237–258. https://doi.org/10.1016/j.jcsr.2014.04.002.

Zhang, S. M., and I. Khan. 2009. "Buckling and ultimate capability of plates and stiffened panels in axial compression." *Mar. Struct.* 22 (4): 791–808. https://doi.org/10.1016/j.marstruc.2009.09.001.